Applied Catalysis B: Environmental 142–143 (2013) 487–493

Contents lists available at SciVerse ScienceDirect

Applied Catalysis B: Environmental

journal homepage: www.elsevier.com/locate/apcatb

Selective oxidation of benzyl alcohol into benzaldehyde over semiconductors under visible light: The case of $Bi_{12}O_{17}Cl_2$ nanobelts

Xiaoyi Xiao, Jing Jiang, Lizhi Zhang*

Key Laboratory of Pesticide & Chemical Biology of Ministry of Education, Institute of Environmental Chemistry, College of Chemistry, Central China Normal University, Wuhan 430079, PR China

ARTICLE INFO

Article history:
Received 4 February 2013
Received in revised form 28 April 2013
Accepted 22 May 2013
Available online 28 May 2013

Keywords:
Selective oxidation
Visible light photocatalysis
Benzyl alcohol
Direct hole oxidation
$Bi_{12}O_{17}Cl_2$ nanobelts

ABSTRACT

In this study we propose several criteria for semiconductor photocatalysts suitable for visible light driven selective oxidation of BA to BAD by employing several literature-reported photocatalysts (P25, g-C_3N_4, $In(OH)_xS_y$, Bi_3O_4Br, BiOBr and Cu_2O) to oxidize BA under visible light, and then demonstrate that the selectivity of photocatalytic oxidation of benzyl alcohol is highly depended on the position of valence band of semiconductors and $Bi_{12}O_{17}Cl_2$ nanobelts could efficiently and selectively oxidize benzyl alcohol into benzaldehyde under visible light via direct hole oxidation. Although the presence of molecular oxygen and the generation of superoxide radicals are important for the selective oxidation of benzyl alcohol, the exact role of molecular oxygen is merely to trap photogenerated electrons to produce superoxide radicals during $Bi_{12}O_{17}Cl_2$ photocatalysis, which could inhibit the recombination of photogenerated charge carries, but might not be involved in the alcohol oxidation directly. The role of molecular oxygen during $Bi_{12}O_{17}Cl_2$ photocatalysis was found to be different from those of TiO_2 and g-C_3N_4 previously reported. This study provides new physical insights for the roles of active species during selective oxidation of alcohol under visible light and the design of novel visible light active photocatalysts for selective oxidation of alcohol.

1. Introduction

The development of green and sustainable organic synthesis methods to partially oxidize alcohols into corresponding aldehydes has gained significant interest [1,2]. Photocatalytic technology is thought to be a reliable, green, and powerful method for the oxidation of alcohols into corresponding aldehydes because of natural abundance of solar energy, benign environmental impact, and sustainability [3–5]. In view of these advantages, scientists have intensively studied photocatalytic selective oxidation of benzyl alcohol (BA) into benzaldehyde (BAD) under UV or visible light irradiation. For instance, in 2008 Palmisano's group delivered a pioneer report on the oxidation of BA into BAD in water on nanostructured rutile TiO_2 with medium pressure mercury lamp irradiation, but found the oxidation selectivity of all these rutile TiO_2 was poor, which was attributed to the influence of crystallinity by these researchers [6]. Zhao and co-workers demonstrated that a coupled system of dye-sensitized TiO_2 and TEMPO could effectively oxidize BA by using oxygen and visible light which avoided the generation of strong, nonselective oxidant hydroxyl radicals and photo-induced holes in their photocatalytic system [7]. Recently, mesoporous graphitic carbon nitride (mpg-C_3N_4) was found to be able to selectively oxidize BA with using oxygen and visible light by Wang and co-workers [8]. This novel metal-free photocatalyst could successfully avoid the environmental contamination caused by the transition-metal complex catalysts. They attributed to the high oxidation selectivity to the catalyst surface basicity and semiconductor functions of mpg-C_3N_4. In despite of these advances on the photocatalytic selective oxidation of BA, the physical insights of the selectivity and conversion rate for photocatalytic oxidation of BA into BAD under visible light are still unclear at present, which seriously limit the further progress of selective oxidation of alcohol.

It is generally accepted that the photo-induced holes, hydroxyl radicals and superoxide radicals are the major active species generated during photocatalysis, which are related to the positions of conduction and valance bands of semiconductors. Although all these active species could initiate the oxidation of BA [7–9], their roles on the overall conversion rate of BA and the selective conversion of BA into BAD under visible light are never clarified in detail.

In this paper, we measured cyclic voltammetry (CV) of benzyl alcohol and benzaldehyde, and employed several literature-reported photocatalysts (P25, g-C_3N_4, $In(OH)_xS_y$, Bi_3O_4Br, BiOBr and Cu_2O) to oxidize BA under visible light. Through above experimental results we could propose several criteria for semiconductor photocatalysts suitable for selective oxidation of BA to BAD under

* Corresponding author. Tel.: +86 27 6786 7535; fax: +86 27 6786 7535.
E-mail address: zhanglz@mail.ccnu.edu.cn (L. Zhang).

0926-3373/$ – see front matter © 2013 Elsevier B.V. All rights reserved.
http://dx.doi.org/10.1016/j.apcatb.2013.05.047

visible light. On the basis of these findings, we turn to seek for desirable semiconductor photocatalysts for the selective oxidation of BA into BAD. After many trials, we luckily find that $Bi_{12}O_{17}Cl_2$ nanobelts could well meet the three criteria and therefore be able to efficiently and selectively oxidize BA into BAD under visible light. Meanwhile, this present study also investigated the active species in the photocatalytic oxidation of BA to BAD over $Bi_{12}O_{17}Cl_2$ nanobelts in detail. Based on all above results, this direct hole induced selective oxidation pathway of BA to BAD over $Bi_{12}O_{17}Cl_2$ photocatalysis has been proposed.

2. Experimental

2.1. Sample preparation

All the reagents were purchased from Chemical Reagent Co., Ltd. (Shanghai, China), and used as received without further purification. In a typical synthesis, 0.4850 g (1 mmol) of $Bi(NO_3)_3{\cdot}5H_2O$ was added slowly into 10 mL of KCl aqueous solution with the Bi/Cl molar ratio of 1. Then a 1 mol/L NaOH aqueous solution was added dropwise to adjust the pH value of the solution to 12.6 under vigorous stirring. After being stirred for 0.5 h at room temperature in air, the pale yellow suspension formed, and then poured into a 25 mL Teflon-lined autoclave until 70% of the autoclave volume was filled. The autoclave was allowed to be heated at 160 °C for 24 h, and then the autoclave was cooled in the air to room temperature. The resulting yellow precipitate was collected and washed with deionized water and ethanol several times, and then dried at 50 °C in air. Moreover, the other photocatalysts g-C_3N_4, $In(OH)_xS_y$, Bi_3O_4Br, BiOBr and Cu_2O were prepared according to previous reports,[10–13] and P25 (nanoscale TiO_2 powder, surface area 50 m^2/g) was purchased from Degussa AG of Germany.

2.2. Characterizations

X-ray powder diffraction (XRD) measurement of $Bi_{12}O_{17}Cl_2$ nanobelts was performed in the reflection mode (Cu Kα radiation, λ = 0.15418 nm) on a Rigaku Ultima III X-ray diffractometer. The morphology and particle sizes were observed with scanning electron microscopy (SEM, JEOL 6700-F) and transmission electron microscopy (TEM, JEOL JSM-2010). The samples of TEM were prepared by dispersing the final powders in ethanol with ultrasonic irradiation and then dropping the dispersion on carbon–copper grids. Furthermore, the obtained powders deposited on copper grid were observed by a high-resolution transmission electron microscope operating at 200 kV. Moreover, UV–vis diffuse reflectance spectrum (DRS) was obtained using a UV–vis spectrometer (Shimadzu UV-2550).

2.3. Cyclic voltammetry (CV) of benzyl alcohol and benzaldehyde

The CV was measured by sweeping at 0.05 V/S in CH_3CN/0.1 mol/L $LiClO_4$/*X* mmol/L benzyl alcohol and CH_3CN/0.1 M $LiClO_4$/*X* mmol/L benzaldehyde (*X* = 0.1, 0.2 and 0.5). A glass carbon disk, a platinum plate and a saturated calomel electrode were as the working, counter and reference electrodes, respectively. The redox potentials of BA and BAD were evaluated from the results of voltammogram analysis.

2.4. Photocatalytic oxidation experiments

Photocatalytic oxidation performance of the as-prepared samples was evaluated by the oxidation of benzyl alcohol in an acetonitrile solution at 50 °C using a 500 W Xe lamp with a 420 nm cut-off filter as the light source. Typically, 50 mg of photocatalyst was suspended in 10 mL of 0.5 mmol/L benzyl alcohol acetonitrile solution in a 20 mL round-bottomed flask. Subsequently, the solution was magnetically stirred for 1 h in the dark to ensure the establishment of an adsorption–desorption equilibrium between the photocatalyst and benzyl alcohol before irradiation. At irradiation time of 8 h, about 2 mL of suspension were collected, and then they were centrifuged and filtered through a 0.22 μm membrane filter. The concentration of benzyl alcohol was recorded by using a high-performance liquid chromatography (HPLC; Shimadzu LC-20A, Japan, TC-C18 reverse phase column, injection volume 10 μL, 0.15% of acetic acid/acetonitrile = 50:50, column temperature: 30 °C, flow rate: 0.6 mL/min, detection wavelength: 254 nm).

2.5. Analysis of photocatalysis mechanism

Triethanolamine and tetrachloromethane were added to the photocatalytic oxidation system in order to find out the active species in the conversion process of BA [14–18]. ESR signals of the radicals spin-trapped by 5,5-dimethyl-1-pyrroline-N-oxide (DMPO) were examined with a Bruker ESP 300A spectrometer.[19–22] The irradiation source was a 500 W xenon lamp with a cutoff filter (λ > 420 nm). The settings for the ESR spectrometer were: center field, 3510.00 G; microwave frequency, 9.79 GHz; power, 5.05 mW.

2.6. Electrochemical measurements

The Mott–Schottky (M–S) experiments were conducted to evaluate the band positions of the as-prepared samples. An electrochemical work station (CHI660B, Shanghai, Inc.) connected to a computer was used in our electrochemical experiment. The photoelectrodes were prepared according to Zhang's paper [23]. Typically, the potential range was −0.5 to +0.2 V with potential steps of 0.05 V at a constant frequency of 997 Hz. An as-prepared $Bi_{12}O_{17}Cl_2$ electrode, a platinum plate and a saturated calomel electrode (SCE) were immersed in the 100 mL of 0.1 mol/L $LiClO_4$ acetonitrile solution as the working, counter and reference electrodes, respectively.

2.7. Photocatalytic oxidation of BA under $^{18}O_2$ isotope-labeled oxygen atmosphere

The experiment conditions of the photocatalytic oxidation of BA under $^{18}O_2$ isotope-labeled oxygen atmosphere were the same as those for $^{16}O_2$. The identification of the oxidation products of BA was conducted on GC-MS (Agilent Technologies, GC6890N, MS 5973) that equipped with a HP-5MS capillary column (FactorFour, 30 m × 0.25 mm × 0.50 m). The column temperature began at 50 °C for 3 min, then increased to 250 °C at 10 °C/min. The temperature of sample injector was maintained at 260 °C. According to the NIST mass spectral database, the products were deduced from MS/MS mode and analyzed by scan mode.

3. Results and discussion

It is known that the generation of hydroxyl radicals and superoxide radicals as well as the oxidation ability of photogenerated holes are strongly related to the positions of conduction and valance bands of semiconductors. To clarify the roles of active species on the selective oxidation of BA into BAD, we first employed several literature-reported photocatalysts (P25, g-C_3N_4, $In(OH)_xS_y$, Bi_3O_4Br, BiOBr and Cu_2O) to oxidize BA under visible light. These photocatalysts are representative and could be classified as five types on the basis of their conduction and valance band positions and the reduction potentials of $O_2/{}^{\bullet}O_2^-$, BA/BAD and BAD/oxidized BAD (Fig. 1). The redox potentials of BA and BAD with different concentrations (0.1, 0.2, and 0.5 mmol/L) were evaluated by

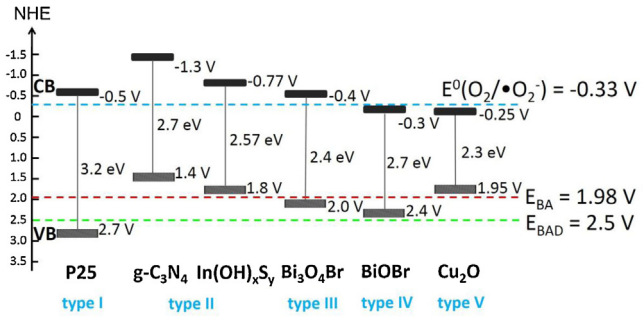

Fig. 1. The schematic diagram of the relationship between the energy band positions of different photocatalysts and the redox potential of BA and BAD.

using cyclic voltammetry, respectively. We found that the redox potentials of BA and BAD were independent on the concentrations (Fig. 2). We define P25 as type I with more negative conduction band than the reduction potentials of $O_2/{}^{\bullet}O_2^-$ and more positive valance band than both of reduction potentials of BA/BAD and BAD/oxidized BAD. $In(OH)_xS_y$ and g-C_3N_4 are defined as type II with more negative conduction band than the reduction potentials of $O_2/{}^{\bullet}O_2^-$, but less positive valance band than both of the reduction potentials of BA/BAD and BAD/oxidized BAD. Bi_3O_4Br is defined as type III with more negative conduction band than the reduction potentials of $O_2/{}^{\bullet}O_2^-$ and more positive valance band than the reduction potentials of BA/BAD, but less positive than that of BAD/oxidized BAD. BiOBr is defined as type IV with less negative conduction band than the reduction potentials of $O_2/{}^{\bullet}O_2^-$ and more positive valance band than the reduction potentials of BA/BAD, but less positive than that of BAD/oxidized BAD. Cu_2O is defined as type V with less negative conduction band than the reduction potentials of $O_2/{}^{\bullet}O_2^-$ and less positive valance band than the reduction potentials of BA/BAD and BAD/oxidized BAD. In this study the reduction potential of •OH/—OH is not considered for the classification because the oxidation of BA is often carried out in non-aqueous solution, resulting in negligible oxidation of —OH to •OH. Moreover, hydroxyl radicals with too strong oxidation ability are thought to be deleterious to the selective oxidation of BA into BAD [8].

Table 1 summarizes the overall conversion rates of BA and the selectivities of BA into BAD over the six photocatalysts under visible light irradiation. The overall conversion rate of BA over P25 was the highest (59.5%), but the corresponding selectivity of BA into BAD was poor (70–85%), which should be attributed to its more positive valance band than the reduction potential of BAD/oxidized BAD. The overall conversion rates of BA over g-C_3N_4 and $In(OH)_xS_y$ were respectively 22.1% and 7.1%, accompanying with more than 99% selectivity of BA into BAD. The overall conversion rate of BA and the selectivity of BA into BAD over Bi_3O_4Br were 36.0% and higher than 99%, respectively. BiOBr could convert 21.6% of BA into BAD with more than 99% selectivity. Because the conduction band of Cu_2O is not negative enough for the generation of superoxide radicals and its valance band is not positive enough for the oxidation of BA via photogenerated holes, we did not observe the oxidation products of BA over Cu_2O under visible light. These results suggest both superoxide radicals and photogenerated holes might contribute to the selective oxidation of BA into BAD. For Fig. 1, we notice that both valance band positions of Bi_3O_4Br and BiOBr are located between the reduction potentials of BA/BAD and BAD/oxidized BAD. Regarding Bi_3O_4Br and BiOBr possess similar element compositions and layer structures interleaved with bismuth-oxide and bromine slabs, we could assume the photogenerated holes of Bi_3O_4Br and BiOBr make the same contribution to the selective oxidation of BA into BAD, 21.6% of BA oxidation could then be assigned to the contribution of photogenerated holes of Bi_3O_4Br among 36% of overall conversion of BA. We therefore estimate that the contribution percentages of superoxide radicals and photogenerated holes to the selective oxidation of BA to BAD over Bi_3O_4Br are 40% and 60%, respectively. For the above results and analysis, we conclude that the valance band position of semiconductors is more crucial for the selective oxidation of BA to BAD and photogenerated holes contribute more to the overall conversion for the two bismuth based photocatalysts. Theoretical calculation reveals that the conduction and valance bands of BiOBr are made up of Bi 6p, O 2p and Br 4p orbital.[31] Bi 6p contribute much to the conduction band, but less to the valance band. Bi_3O_4Br possesses similar composition of band structure with BiOBr, but the intensity of Bi 6p orbital in CB bottom of Bi_3O_4Br is stronger than that of BiOBr, suggesting a more negative conduction band of

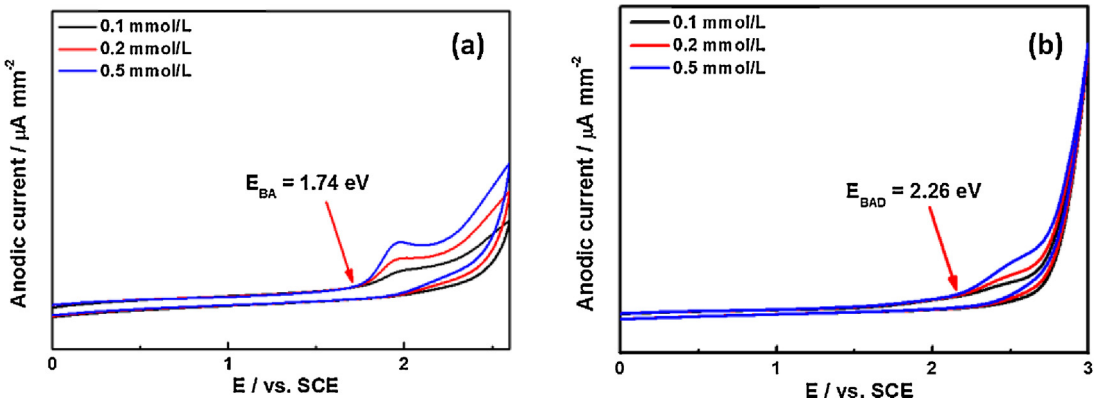

Fig. 2. The cyclic voltammogram of benzyl alcohol (a) and benzaldehyde (b) with different concentrations (0.1, 0.2, and 0.5 mmol/L).

Table 1
Conversion rates and selectivity of BA oxidation into BAD over different photocatalysts.

Photocatalyst	P25	g-C_3N_4	$In(OH)_xS_y$	Bi_3O_4Br	BiOBr	Cu_2O
Conversion rates (%)	59.5	22.1	7.1	36.0	21.6	0
Selectivity (%)	70–85	>99	>99	>99	>99	0

In a typical reaction, 50 mg of catalysts were added to 10 mL of acetonitrile in a 20 mL round bottom flask. The O_2 source was introduced and the closed round bottom flask was heated to 50 °C by water bath, followed by visible light irradiation for 8 h.

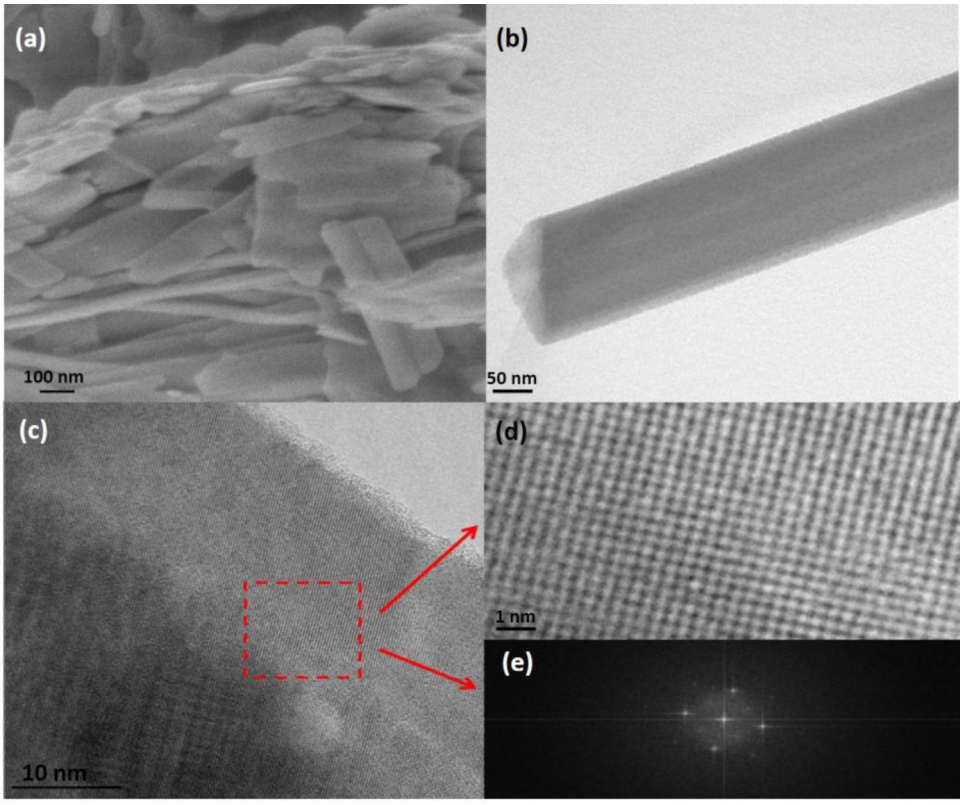

Fig. 3. (a) SEM image; (b) TEM image; (c and d) HR-TEM images; and (e) SAED pattern of the as-prepared $Bi_{12}O_{17}Cl_2$ nanobelts.

Bi_3O_4Br. The more negative conduction band of Bi_3O_4Br enables photogenerated electrons to react with molecular oxygen to produce superoxide radicals for the enhanced selective oxidation of BA to BAD, consistent with the aforementioned experimental results.

On the basis of the above results, we could propose several criteria for semiconductor photocatalysts suitable for selective oxidation of BA to BAD under visible light as follows. (1) The conduction band position should be more negative than the reduction potential of $O_2/{}^{\bullet}O_2^-$ (−0.33 V) [24,25]; (2) the valance band position should be located between the reduction potentials of BA/BAD and BAD/oxidized BAD (1.98–2.50 V); (3) the band gap energy should be just slightly larger than 2.31 eV in view of better utilization of solar energy. On the basis of these finding, we turn to seek for desirable semiconductor photocatalysts for the selective oxidation of BA into BAD. After many trials, we luckily find that $Bi_{12}O_{17}Cl_2$ nanobelts could well meet the three criteria and therefore be able to efficiently and selectively oxidize BA into BAD under visible light.

$Bi_{12}O_{17}Cl_2$ nanobelts were synthesized via a mild hydrothermal treatment of $Bi(NO_3)_3{\cdot}5H_2O$ and KCl in NaOH aqueous solution. X-ray diffraction (XRD) analysis revealed the as-prepared sample was well crystallized and phase-pure. The sample could be well indexed to the tetragonal structures of $Bi_{12}O_{17}Cl_2$ (JCPDS File No. 37-702). Scanning electron microscopy (SEM) and transmission electron microscopy (TEM) analyses showed that the as-prepared sample consisted of numerous belts with length of 400 to more than 1000 nm and width of 50–100 nm (Fig. 3a and b). High-resolution TEM (HRTEM) images (Fig. 3c and d) revealed the highly crystalline nature of the $Bi_{12}O_{17}Cl_2$ nanobelts. Furthermore, the clear lattice spacing was about 0.27 nm between adjacent lattice planes of the as-prepared sample, consistent with the *d*-spacing of the [2 0 0] planes [26]. The selected-area electron diffraction (SAED) pattern (Fig. 3e) revealed the single-crystalline characteristic of the $Bi_{12}O_{17}Cl_2$.

UV–vis diffuse reflectance spectrum (DRS) of $Bi_{12}O_{17}Cl_2$ nanobelts is shown in Fig. 4. It is found that the optical absorption of $Bi_{12}O_{17}Cl_2$ nanobelts from UV light to visible light and the absorption edge of $Bi_{12}O_{17}Cl_2$ nanobelts is up to 530 nm. As a crystalline semiconductor, the optical absorption near the band edge follows the formula $\alpha h\nu = A(h\nu - E_g)^{n/2}$, where α, ν, E_g, and A are the absorption coefficient, light frequency, band gap energy, and a constant, respectively [27–29]. In addition, n is a constant that depends on the characteristics of the transition in the semiconductor, namely, direct transition ($n = 1$) or indirect transition ($n = 4$). The optical transition for $Bi_{12}O_{17}Cl_2$ nanobelts was indirect and

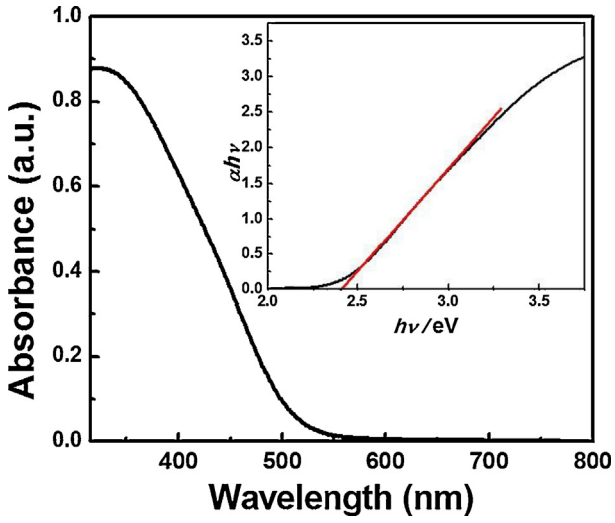

Fig. 4. UV–vis diffuse reflection spectrum and $\alpha h\nu$–$h\nu$ curve (inset) of the as-prepared $Bi_{12}O_{17}Cl_2$ nanobelts.

Table 2
Comparisons of BA oxidation over $Bi_{12}O_{17}Cl_2$ nanobelts under different reaction conditions[a].

	Solvent	Catalyst	$h\nu$	O_2 source	Con. (%)[b]	Sel. (%)
1	Acetonitrile	+	+	Air	41	>99
2	Acetonitrile	+	+	O_2	44	>99
3[c]	Acetonitrile	+	+	–	33	>99
4[d]	Acetonitrile	+	–	Air	<1	–
5[e]	Acetonitrile	–	+	Air	<1	–

[a] In a typical reaction, 50 mg of $Bi_{12}O_{17}Cl_2$ was added to 10 mL of acetonitrile in a 20 mL round bottom flask. The O_2 source was introduced and the closed round bottom flask was heated to 50 °C by water bath, followed by visible light irradiation for 8 h.
[b] Conversion rates were determined by HPLC.
[c] Reference experiment in the absence of O_2.
[d] Reference experiment without visible light irradiation.
[e] Reference experiment without $Bi_{12}O_{17}Cl_2$.

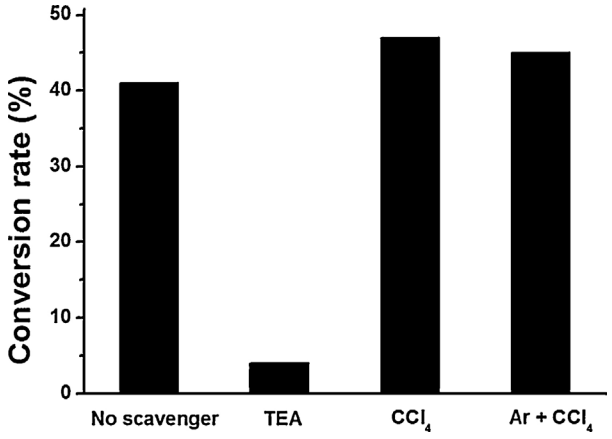

Fig. 5. The conversion of BA over $Bi_{12}O_{17}Cl_2$ nanobelts by adding different scavengers under visible light.

the band gap energy of $Bi_{12}O_{17}Cl_2$ nanobelts was estimated to be 2.43 eV (inset of Fig. 4).

The as-prepared $Bi_{12}O_{17}Cl_2$ nanobelts were then used to oxidize BA under visible light. We found that 41.0% of BA (Table 2, entry 1) could be selectively oxidized into BAD under visible light with using air. Meanwhile, BA could not be converted into BAD in the absence of either the light source or the photocatalyst (Table 2), suggesting the conversion of BA over $Bi_{12}O_{17}Cl_2$ nanobelts was proceeded via a photocatalytic process. To understand the role of molecular oxygen during the selective oxidation of BA into BAD over $Bi_{12}O_{17}Cl_2$ nanobelts under visible light, we purged out air with Ar during photocatalysis and found that the conversion of BA was decreased slightly to 33.0% in case of Ar, confirming that molecular oxygen in air does contribute to the selective oxidation of BA into BAD, but just with about 19.5% of contribution among the overall conversion (Table 2, entry 3). However, the conversion rate of BA (44.0%) in oxygen atmosphere only slightly increased in comparison with air atmosphere (Table 2, entry 2), suggesting the dioxygen in air was sufficient for this photocatalytic conversion reaction.

A series of active species trapping experiments were further conducted to further investigate the photocatalytic oxidation mechanism of BA into BAD. When triethanolamine (TEA) was added to the BA system to trap the holes [17,18], the conversion rate of BA decreased significantly (Fig. 5), revealing that the photogenerated holes are the major oxidative species for the selective oxidation of BA into BAD. The addition of electron scavenger tetrachloromethane could slightly increase the conversion of BA (Fig. 5) [14–16], further confirming that the photogenerated holes were crucial for the oxidation of BA. When we removed molecular oxygen with Ar in the presence of tetrachloromethane, the conversion rate of BA into BAD surprisingly increased, suggesting the trapping of photogenerated electrons with tetrachloromethane could

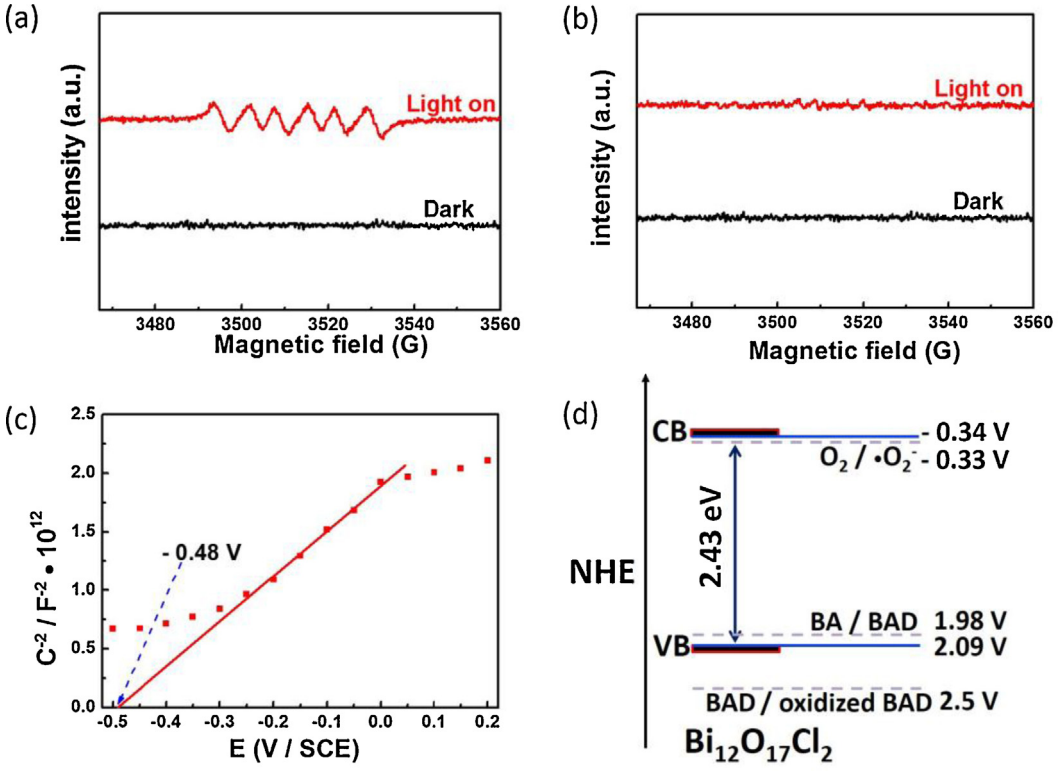

Fig. 6. (a) DMPO spin-trapping ESR spectra of $Bi_{12}O_{17}Cl_2$ nanobelts in methanol dispersion for DMPO–$^{\bullet}O_2^-$, (b) DMPO spin-trapping ESR spectra of $Bi_{12}O_{17}Cl_2$ acetonitrile dispersion for DMPO–$^{\bullet}$OH, (c) Mott–Schottky plots for the $Bi_{12}O_{17}Cl_2$ electrodes, and (d) estimated band positions of $Bi_{12}O_{17}Cl_2$ nanobelts.

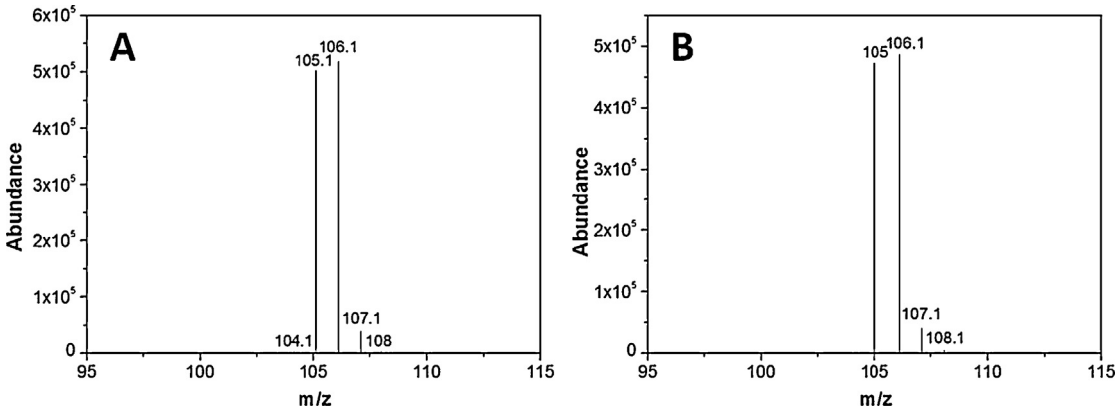

Fig. 7. The mass spectra of the benzaldehyde produced in different atmosphere. (A) The mass spectra of the benzaldehyde produced in $^{16}O_2$ atmosphere. (B) The mass spectra of the benzaldehyde produced in $^{18}O_2$ atmosphere.

benefit the photogenerated hole induced selective oxidation of BA to BAD and superoxide radicals is not essential for the selective oxidation of BA to BAD over $Bi_{12}O_{17}Cl_2$ nanobelts under visible light. These active species trapping experimental results suggest that the role of molecular oxygen is to trap photogenerated electrons to produce superoxide radicals, while the formation of superoxide radicals could inhibit the recombination of photogenerated charge carries, which favor the selective oxidation of BA to BAD induced by the photogenerated holes on the valance band of $Bi_{12}O_{17}Cl_2$ nanobelts. ESR with DMPO spin-trap technique was carried out to identify the generation of reactive oxygen species (ROSs). Fig. 6a reveals six characteristic signals of DMPO–$^{\bullet}O_2^-$ adduct generated over $Bi_{12}O_{17}Cl_2$ nanobelts in the acetonitrile solution under visible light [21], confirming the formation of superoxide radicals. Four characteristic peaks of DMPO–$^{\bullet}$OH adduct were not observed either in the dark or in the visible light irradiated $Bi_{12}O_{17}Cl_2$ methanol dispersion (Fig. 6b) [22], ruling out the generation of hydroxyl radical.

Mott–Schottky experiment was conducted to evaluate the band positions of the as-prepared $Bi_{12}O_{17}Cl_2$ nanobelts (Fig. 6c). We found that the slope of linear $1/C^2$ potential curve was positive, indicating that $Bi_{12}O_{17}Cl_2$ has an n-type semiconductor characteristic. The flat band potential of $Bi_{12}O_{17}Cl_2$ nanobelts was −0.48 V vs SCE (0.24 V vs NHE). It is known that the bottom of the conduction bands was more negative by ~−0.1 V than the flat band potential for many n-type semiconductors [30]. Therefore, the estimated positions of conduction and valence bands of $Bi_{12}O_{17}Cl_2$ nanobelts are −0.34 and 2.09 V vs NHE, respectively. Fig. 6d presents the positions of conduction and valence bands of $Bi_{12}O_{17}Cl_2$ nanobelts as well as the reduction potentials of $O_2/^{\bullet}O_2^-$, BA/BAD and BAD/oxidized BAD, which reveals that $Bi_{12}O_{17}Cl_2$ nanobelts could well meet our proposed three criteria and therefore be an attractive visible light active photocatalyst for selective oxidation of benzyl alcohol.

To further clarify the exact role of molecular oxygen during $Bi_{12}O_{17}Cl_2$ photocatalysis, the photocatalytic oxidation of BA under ^{18}O isotope-labeled oxygen atmosphere was performed in acetonitrile solution. We could not detect any ^{18}O-labeled BAD produced during $Bi_{12}O_{17}Cl_2$ photocatalysis (Fig. 7), ruling out the direct participation of molecular oxygen and ROSs in the oxidation of BA. This observation is different from the case of selective oxidation of BA over TiO_2 under UV light, which involves an oxygen atom transfer from the dioxygen to the a-carbon atom of the alcohol [9]. This difference might be ascribed to more difficult formation of Bi—O—O bond than that of Ti—O—O bond, which needs further investigation. The oxygen isotope experimental results confirm that the role of molecular oxygen is merely to trap photogenerated electrons to produce superoxide radicals, which could inhibit the recombination of photogenerated charge carries, but not be directly involved in the oxidation of BA to BAD during $Bi_{12}O_{17}Cl_2$ photocatalysis.

On the basis of the above results and analysis, we propose a possible pathway of benzyl alcohol selective oxidation over $Bi_{12}O_{17}Cl_2$ nanobelts under visible light (Scheme 1). First, $Bi_{12}O_{17}Cl_2$ nanobelts are excited under visible light and produce plenty of photogenerated carriers and benzyl alcohol is deprotonated to form alkoxide anions. The electrons on the conduction band would be

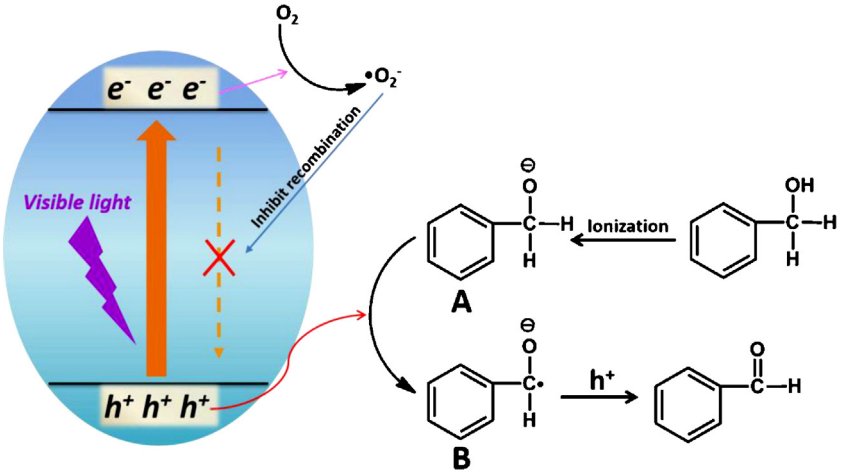

Scheme 1. Proposed reaction mechanism for the photocatalytic selective oxidation of benzyl alcohol over $Bi_{12}O_{17}Cl_2$ nanobelts under visible light.

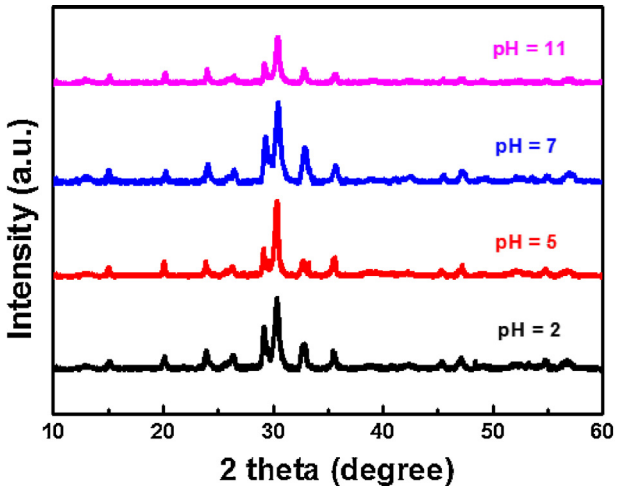

Fig. 8. XRD patterns of $Bi_{12}O_{17}Cl_2$ after being suspended in aqueous solutions with different pH values (from 2 to 11).

trapped by electrophilic O_2, leaving photogenerated holes on the valance band. Then the alkoxide anions would react with the photogenerated holes and subsequently deprotonate to form carbon radicals. The carbon radicals further react with photogenerated holes to release electrons to form benzaldehyde. Obviously, this direct hole induced selective oxidation pathway of BA to BAD over $Bi_{12}O_{17}Cl_2$ photocatalysis is obviously not the same either as that of TiO_2 photocatalysis with an oxygen atom transferred from the molecular oxygen to the a carbon atom of the alcohol [9], or as that of mpg-C_3N_4 photocatalysis involving the reaction of carbon radicals with superoxide radicals [8].

We evaluated the stability of the as-prepared photocatalyst after being suspending in the solution with different pH values (from 2 to 11) and found the photocatalyst could be stable at different pH values (Fig. 8), suggesting its potential for application.

4. Conclusion

In conclusion, we have demonstrated that the selectivity of photocatalytic oxidation of benzyl alcohol is highly depended on the position of valence band of semiconductors and $Bi_{12}O_{17}Cl_2$ nanobelts could efficiently and selectively oxidize benzyl alcohol into benzaldehyde under visible light via direct hole oxidation. Although the presence of molecular oxygen and the generation of superoxide radicals are important for the selective oxidation of benzyl alcohol, the exact role of molecular oxygen is only to be a photogenerated electron scavenger to produce superoxide radicals to inhibit the recombination of photogenerated charge carries during $Bi_{12}O_{17}Cl_2$ photocatalysis. The generated superoxide radicals might not participate in the oxidation of BA over $Bi_{12}O_{17}Cl_2$ nanobelts under visible light. This study provides new physical insights for the roles of active species during selective oxidation of alcohol under visible light and the design of novel visible light active photocatalysts for selective oxidation of alcohol.

Acknowledgements

This work was supported by National Basic Research Program of China (973 Program) (Grant 2013CB632402), and National Science Foundation of China (Grants 21073069, 91023010, and 21177048).

References

[1] A. Baiker, T. Mallat, Chemical Reviews 104 (2004) 3037–3058.
[2] J.A. Mueller, C.P. Goller, M.S. Sigman, Journal of the American Chemical Society 126 (2004) 9724–9734.
[3] K. Honda, A. Fujishiam, Nature 238 (1972) 38–39.
[4] D.A. Nicewicz, D.W.C. Macmillan, Science 322 (2008) 77–80.
[5] M.S. Ischay, M.E. Anzovino, J. Du, T.P. Yoon, J. Am. Chem. Soc. 130 (2008) 12886–12887.
[6] S. Yurdakal, G. Palmisano, V. Loddo, V. Augugliaro, L. Palmisano, Journal of the American Chemical Society 130 (2008) 1568–1569.
[7] M. Zhang, C.C. Chen, W.H. Ma, J.C. Zhao, Angewandte Chemie International Edition 120 (2008) 9876–9879.
[8] F.Z. Su, S.C. Mathew, G.L. Lipner, X.Z. Fu, M. Antonietti, S. Blechert, X.C. Wang, Journal of the American Chemical Society 132 (2010) 16299–16301.
[9] M. Zhang, Q. Wang, C.C. Chen, L. Zang, W.H. Ma, J.C. Zhao, Angewandte Chemie International Edition 48 (2009) 6081–6084.
[10] G.H. Dong, L.Z. Zhang, Journal of Materials Chemistry 22 (2012) 1160–1166.
[11] S.X. Ge, L.Z. Zhang, Environmental Science and Technology 45 (2011) 3027–3033.
[12] H. Deng, J.W. Wang, Q. Peng, X. Wang, Y.D. Li, Chem. Eur. J. 11 (2005) 6519–6524.
[13] Y.B. Cao, J.M. Fan, L.Y. Bai, F.L. Yuan, Y.F. Chen, Crystal Growth and Design 10 (2010) 232–236.
[14] J.E. Chateauneuf, Journal of the American Chemical Society 112 (1990) 442.
[15] M. Washio, Y. Yoshido, N. Hayashi, H. Kobayashi, S. Tagawa, Y.R. Tabata, Phys. Chem. 34 (1989) 115.
[16] A. Saeki, N. Yamamoto, Y. Yoshida, T. Kozawa, Journal of Physical Chemistry A 115 (2011) 10166–10173.
[17] S.C. Yan, Z.S. Li, Z.G. Zou, Langmuir 26 (2010) 3894–3901.
[18] X.C. Wang, K. Maeda, A. Thomas, K. Takanabe, G. Xin, J.M. Carlsson, K. Domen, M. Antonietti, Nature Materials 8 (2009) 76.
[19] T.J. Yan, J.L. Long, X.C. Shi, D.H. Wang, Z.H. Li, X.X. Wang, Environmental Science and Technology 44 (2010) 1380–1385.
[20] N. Zhang, X.Z. Fu, Y.J. Xu, J. Mater. Chem. 21 (2011) 8152–8158.
[21] Y.H. Zhang, Z.R. Tang, X.Z. Fu, Y.J. Xu, ACS Nano 5 (2011) 7426–7435.
[22] J.H. Huang, Y.D. Hou, X.F. Chen, L. Wu, X.C. Wang, X.Z. Fu, Environmental Science and Technology 42 (2008) 7387–7391.
[23] Y.J. Zhang, T. Mori, J.H. Ye, M. Antonietti, Journal of the American Chemical Society 132 (2010) 6294–6295.
[24] A. Ishikawa, T. Takata, J.N. Kondo, M. Hara, H. Kobayashi, K. Domen, J. Am. Chem. Soc. 124 (2002) 13547–13553.
[25] R. Abe, H. Takami, N. Murakami, B. Ohtani, Journal of the American Chemical Society 130 (2008) 7780–7781.
[26] X.Y. Chen, H.S. Huh, S.W. Lee, Journal of Solid State Chemistry 180 (2007) 2510–2516.
[27] M.A. Butler, Journal of Applied Physics 48 (1977) 1914–1920.
[28] J.W. Tang, Z.G. Zou, J.H. Ye, Journal of Physical Chemistry B 107 (2003) 14265–14269.
[29] S.M. Sun, W.Z. Wang, L. Zhang, L. Zhou, W.Z. Yin, M. Shang, Environmental Science and Technology 43 (2009) 2005–2010.
[30] A. Ishikawa, T. Takata, J.N. Kondo, M. Kara, H. Kobayashi, K. Domen, Journal of the American Chemical Society 124 (2002) 13547–13553.
[31] H.J. Zhang, L. Liu, Z. Zhou, Physical Chemistry Chemical Physics 14 (2012) 1286–1292.